

Final As-revised

MD Description of Damage Production in Displacement Cascades in Copper and α -Iron

D.J. Bacon^{1*}, Yu.N. Osetsky¹, R. E. Stoller² and R.E. Voskoboinikov¹

¹ Materials Science and Engineering, Department of Engineering,
The University of Liverpool, Brownlow Hill, Liverpool L69 3GH, UK.

² Oak Ridge National Laboratory, P.O. Box 2008, Oak Ridge, TN 37831-6158, USA.

* corresponding author: djbacon@liv.ac.uk

ABSTRACT

Molecular dynamics computer simulation has been applied for an extensive study of primary damage creation in displacement cascades in copper and α -iron. Primary knock-on atom energy, E_p , of up to 25keV in copper and 100keV in iron has been considered for irradiation temperatures in the range 100 to 900K. Special attention has been paid to comprehensive statistical treatment of the number and type of defects created in cascades by conducting multiple simulations for each value of energy and temperature. The total number of point defects per cascade is significantly lower than that predicted by the NRT model and rather similar in the two metals. The fraction of self-interstitial atoms (SIAs) and vacancies that agglomerate in clusters in the cascade process has been analysed in detail. The clustered fraction of SIAs increases with increasing temperature and is larger in copper than iron. SIA clusters have a variety of forms in both metals and, although most are glissile clusters of parallel crowdions, a significant fraction are sessile. The latter include Frank dislocation loops in copper. Tightly-packed arrangements of vacancies do not form in iron, and so the fraction of clustered vacancies depends strongly on the range within which defects are defined to be near-neighbours. Arrangements of vacancies in first-neighbour sites are common in copper. Most are irregular stacking fault tetrahedra (SFTs). In 53 simulations of cascades with $E_p = 25\text{keV}$ at 100K, the largest cluster formed contained 89 vacancies. The size spectrum of SFT-like clusters is similar to that found experimentally in neutron-irradiated copper, suggesting that the SFTs observed in experiment are formed directly in the cascade process.

1. Introduction

Candidate materials for structural components of fusion reactor systems must be assessed for their ability to operate at high temperature under high fluxes of fast neutrons without exhibiting a significant degradation of service properties. They will need to withstand radiation damage processes that occur over wide ranges of length and time scales, i.e. from defect production at the atomic-level ($\sim 10^{-15}$ s, 10^{-10} m) to microstructural evolution over the mesoscale ($\sim 10^6$ s, 10^{-3} m). In order to achieve progress in predictive modelling of property changes across these scales, atomic-scale computer simulation occupies a special place, for it is able to provide much of the input to models at the higher levels. Large strides have been made over the past decade as a result of the increasing power of computational facilities and in this paper we present results obtained recently with regard to two pure metals, namely copper and α -iron. This will enable us to point to more general features of metals with FCC and BCC crystal structures.

We consider displacement cascades. They are the primary source of radiation damage during fast-neutron irradiation of metals and are formed by the recoil of primary knock-on atoms (PKAs) with a kinetic energy of more than ~ 1 keV. The cascade process is characterised by lengths and times of the order of nm and ps, respectively, and it cannot be investigated directly by either experimental or analytical techniques. Only atomic-scale computer simulation by method of molecular dynamics (MD) is suitable for studying the creation of point defects - see reviews [1-4] and references cited therein - and their stability, mobility and interaction. The latter features are important because point defects cluster directly in the cascade process and the properties of the clusters have important consequences for microstructure evolution and property changes under cascade damage conditions [5,6]. However, most studies of cascade simulation using MD have only treated a few (typically ≤ 5) cascades at a given energy, and so firm statistics on cluster type and size distribution, particularly as needed for computational models of damage evolution, are lacking. Also, and possibly for the same reason, there seems to be an insufficiency of cluster types observed in these cascade simulations, so that it is not easy to compare results of modelling with experimental data. For example, low- and high-temperature experiments on copper have shown efficient production of stacking fault tetrahedra (SFTs) [7-9], but, with the exception of a preliminary report of our work [10], they have not been observed systematically in cascade simulation. This is rather surprising because MD simulations of the evolution of a hot, vacancy-rich zone have demonstrated effective formation of SFT under this

condition [11-13]. Thus, we are undertaking an in-depth study of cascades in copper, an FCC metal with low stacking fault energy in which SFTs are observed. Further, in this paper we compare simulations for copper with those for BCC iron, for previous (less numerous) simulations in a lower PKA energy regime have shown that differences in defect number and cluster population may be expected between these two metals [14].

2. Simulation Models

Two interatomic potentials were used for copper, namely an equilibrium, short-ranged, many-body potential (MBP) [15] and a non-equilibrium, long-ranged pair potential (PP) [16]. Both were modified at short distance by fitting to a screened Coulomb potential following the Biersack formulation [17]. Plots of the effective pair form of these potentials are presented in [18]. The PP describes a slightly bigger effective size of ion, which leads to an average threshold displacement energy, E_d , of 42eV, which is higher than 28eV obtained with the MBP. The potential used for α -iron is the many-body potential of Finnis and Sinclair [19], again modified in the pair part for short-range interactions by a screened Coulomb function [20].

PKAs in $\langle 135 \rangle$ directions with energy in the range up to 25keV in copper and 100keV in iron were simulated at ambient temperatures of 100 and 600K in cubic crystallites containing up to 2,000,000 (copper) and 10,000,000 (iron) mobile atoms with periodic boundary conditions. The larger size was used consistently for the 25keV cascades in copper: this avoided the necessity to terminate and thus exclude simulations of widely-spread cascades, which proved necessary for some cascades in iron (see, for example, [21]). No treatment of electron-phonon coupling was applied and heat was not extracted from the crystallite during cascade evolution. Monitoring of temperature and its distribution in the crystallite showed that after cascade relaxation the mean temperature increased by a maximum of ~ 100 K for the ranges of energy and crystallite size considered. This increase does not materially affect the final result within the time of simulation. We found that overestimation of the MD time step in the early collision stage tends to result in denser cascades, more defect clustering and a larger number of surviving defects. To avoid this, we used a variable time-step integration in the MD loop of between 0.01 and 5fs for iron and 0.003 to 4.5fs for copper [10, 22].

Finally, as noted earlier, a prime reason for modelling copper was to generate enough cascades for conclusions to be drawn with a firm statistical basis and to allow meaningful comparisons with experiment. Thus, for this metal, a large number (maximum up to 53) of cascades, of the same energy and temperature were simulated for the same conditions in order to allow a wide variety of defects to form and be analysed.

3. Defect numbers

The number, N_F , of surviving defects at the end of the cascade process (i.e. the number of self-interstitial atoms (SIAs) or vacancies) versus PKA energy, E_p , for the two metals modelled using the MBPs are presented in Fig. 1. The results plotted are the mean and standard error (SE) from the MD data for N_F at each energy, normalised to the value, N_{NRT} , predicted by the standard formula [23]:

$$N_{NRT} = 0.8E_{dam}/2E_d, \quad (1)$$

where E_{dam} is the energy available for damage by displacements, which is E_p in the MD modelling, and E_d is the mean threshold energy for creating a stable Frenkel pair. With the ASTM-recommended standard values for E_d of 30 and 40eV for copper and iron, respectively, N_{NRT} for these two metals is $13.3E_p$ and $10E_p$ when E_p is expressed in keV. The N_F data plotted for copper is for simulations at 100K, whereas that for iron is for all the temperatures considered. However, the values of N_F for iron are relatively insensitive to temperature, a result found earlier in a comparison of simulation data for the two metals for E_p up to 10keV [14], and in results of other simulations of copper [10], iron [24], zirconium [25] and the ordered alloy Ni_3Al [26]. The NRT-normalised values of N_F fall between about 0.15 and 0.2 for copper and 0.3 to 0.4 for iron at PKA energies above a few keV. This is again consistent with the low-energy data presented in [14], but the apparent difference is largely a consequence of the choice of E_d used in the normalisation. This is clear from comparing the mean values of N_F for both metals at 100K in Figs. 2(a) and (b). These plots also contain the SE and standard deviation (SD) bars for each E_p . It can be seen that although the SE is small, the SD is rather large, implying that the data on N_F are distributed with large dispersion and are statistically not well-defined. This is clear from Fig. 2(b), where all the N_F values for copper are plotted. (The same effect occurs at all temperatures,

as typified by the data for 20keV cascades in copper at 600K included in Fig. 2(b).) Thus, more cascade simulations are necessary to investigate the full distribution of N_F comprehensively. The scales of both ordinate and abscissa in these figures are chosen to be logarithmic in order to test the validity of the power-law formulation $N_F = A(E_p)^m$, which was found in [2] to give a good fit to data from MD simulations with $m \approx 0.75$, instead of the value $m = 1$ in the NRT formula, for cascades with $E_p \leq 10$ keV. The low energy results from the present work can be fitted well with the parameters A and m discussed earlier [2,3], whereas higher energy cascades give a value of m close to 1, as first reported for iron in ref. [21] and found to be due to the higher probability of subcascade formation.

4. Defect cluster formation

The large number of events simulated resulted in a wide variety of defect structures. In both metals, a general trend of an increasing fraction of defects in clusters (and therefore of maximum cluster size) with increasing PKA energy was observed. However, it should be noted that in any particular cascade the fraction of clustered defects, $\varepsilon = N_c/N_F$, where N_c is the number of defects in clusters containing two or more, was found to deviate significantly from the mean. For example, for 20keV cascades simulated at 100K with the MBP for copper, ε varied from 0.12 to 0.77. Simulations where significant clustering was observed usually created the largest number of surviving defects, indicating that clustering effects and the number N_F are correlated. (A summary on maximum cluster size and the corresponding number of surviving defects for both SIAs and vacancies was given for the MBP and PP models of copper in table 1 of reference [10].) We now present the cluster statistics and cluster configurations formed in the cascade process in more detail, starting with the SIAs.

4.1. Interstitial clusters

(a) Fraction of SIAs in clusters

Interstitial clusters have a relatively high binding energy per defect, and it is appropriate to identify an SIA as part of a cluster if it has at least one other interstitial in a nearest neighbour position. Histograms showing the mean values of the fraction of the SIA population in clusters

of a given size at 100K for cascades of either 10 and 50keV in iron or 10 and 25keV in copper are plotted in Figs. 3(a) and (b), respectively. Clearly, the population skews towards the larger clusters with increasing PKA energy in both metals. It is also seen that the fraction of defects in clusters containing two or more is larger in copper than iron, as first found for lower energy cascades by Phythian et al. [14]. The effect of increasing the ambient temperature, whilst small as far as N_F is concerned, is to change the clustered fraction of SIAs, ϵ_i , more significantly. Although the effect was reported to be small for iron at low cascade energy ($\leq 5\text{keV}$) in references [14,24], the mean ϵ_i for about 10 cascades at 20keV increases from 0.61 to 0.75 as temperature increases from 100 to 600K [21]. (A similar increase of 10-15% was reported for ϵ_i in zirconium as temperature is increased from 100 to 600K for cascades of up to 20keV [25].) In the present study with much stronger statistics, the data for copper show quite clearly that ϵ_i increases strongly with temperature as well as PKA energy. This is demonstrated by the ϵ_i data for the PP model of copper in Fig. 4.

The sensitivity of the data for the SIA cluster fraction to choice of interatomic potential has been tested by calculating the mean of ϵ_i for simulations at 100K for the MBP model. The data plotted in Fig. 5 shows that this model results in higher values of ϵ_i than those obtained with the PP. Hence, it is necessary to exercise caution in choosing data for ϵ_i , say, on the basis of MD simulations obtained using just one interatomic potential. From the present work, it is safe to say that the mean values of ϵ_i lie between 0.3 and 0.6 for cascades in copper with energy above about 10keV.

One final point needs to be made before closing the discussion on SIA clusters. The data presented in Figs. 4 and 5 for the clustered fraction, ϵ_i , were derived for a minimum cluster size of two interstitials. However, this disguises the sensitivity of the relationship between ϵ_i and E_p to this minimum size, because low-energy cascades in particular do not produce large clusters (see Figs. 2 and 3). This effect may have important consequences in the light of the evidence from MD that the dimensionality of the motion of clusters depends on their size, i.e. clusters of size three or less can change their glide direction and hence migrate three-dimensionally (see subsection (c) below), and this controls the kinetics of their interaction with other components of the microstructure [6]. To illustrate the influence of PKA energy on the fraction of SIAs in three- or one-dimensional clusters, we present in Fig. 6 values for ϵ_i versus E_p in copper at 100

K for the cases where the minimum cluster size is either two, three or four SIAs. It is seen that ε_i is very sensitive to the choice of minimum cluster size in the lower part of the energy spectrum in copper. The data demonstrates the way in which atomic-scale modelling is able to provide detailed information for use in models of damage evolution.

(b) Glissile SIA clusters

Most of the clustered SIAs formed in cascades in metals simulated by MD have the form of densely-packed, parallel crowdions, with the crowdion axis usually along the close-packed direction. They are small, perfect dislocation loops with Burgers vector \mathbf{b} along the crowdion axis, i.e. $\mathbf{b} = 1/2\langle 110 \rangle$ in FCC, $1/2\langle 111 \rangle$ in BCC and $1/3\langle 11\bar{2}0 \rangle$ in HCP. Such a loop is ‘glissile’, for it can glide on the prism defined by its periphery and Burgers vector. The motion of glissile SIA clusters containing up to 121 SIAs (copper) and 337 SIAs (iron) has been investigated by MD using several interatomic potentials, e.g. [27-32]. These clusters exhibit thermally-activated, one-dimensional glide along the crowdion direction and only small clusters (< 4 SIAs) can change their glide direction during the period of MD simulation (~5ns). Their motion cannot be described as classical diffusion [29, 32], but some dynamical characteristics have been estimated by analysing the movement of the centre of gravity of the SIAs in moving clusters. The effective correlation factor is greater than 1, i.e. a cluster that has moved by one step in one direction has a high probability of making the next step in the same direction. This effect increases at low temperature and is probably related to the response of crowdion clusters to specific phonons [29]. Analysis of the jump frequency versus reciprocal temperature gives an effective ‘activation energy’ in the range 0.022-0.026 eV for all clusters in both metals and is close to the migration energy estimated for the low-temperature single crowdion mechanism. Perfect dislocation loops with $\mathbf{b} = \langle 100 \rangle$ can also occur in BCC metals, and a cluster of $\langle 100 \rangle$ crowdions behaves in a similar fashion to a $1/2\langle 111 \rangle$ loop, but with a slightly higher activation energy (0.028 eV) [29,32].

The data for α -Fe have been analysed by Barashev et al. [33], who have shown that the jump frequency of a cluster is approximately equal to the average jump frequency of an individual crowdion in the cluster divided by the number of crowdions. This is consistent with the interpretation that the movement of the centre of mass of an SIA cluster is the result of near-

independent jumps of the individual crowdions in a cluster with high binding energy. However, it should be stressed that there is more complexity in the mobility of SIA clusters in terms of size than represented in this simple picture. For example, when perfect loops with $\mathbf{b} = 1/2\langle 110 \rangle$ in Cu grow beyond about 64 interstitials, they dissociate on their glide prism and the stair-rod partial dislocations formed at the corners restrict thermally-activated motion, and totally prevent it for sizes above 121 SIAs [30-32]. A similar effect cannot occur in Fe because of the absence of a stable stacking fault.

(c) Non-glissile SIA clusters

Not all clusters have the glissile behaviour outlined above, for immobile or ‘sessile’ clusters have been found in the debris of cascades created in MD simulations in a range of metals. They have two basic forms. In BCC metals such as iron, which we consider first, stable stacking faults do not exist and the form of metastable sessile clusters formed in cascades is more diverse. Some arise from the attraction of mobile species that impinge on each other in positions that prevent instantaneous agglomeration into a glissile cluster: others, possibly with the same number of defects, adopt a more open, three-dimensional (3-D) structure. They have a similar size distribution to the glissile loops. Their population and properties have been studied by MD for cascades with energy between 5 and 40 keV in α -iron at 100 and 600K [34]. The mean values of the fraction of interstitials that formed in immobile clusters are plotted as a function of cascade energy in Fig. 7, where the bars denote the SE. Between 30 and 50% of the clustered population have sessile character at an irradiation temperature of 100K: the fraction is reduced by about half at 600K. If immobile clusters of defects were to persist over long time-scales, they could have possibly important consequences for damage evolution, and so their stability was investigated by annealing representative ones individually by MD for long periods (≥ 1 ns) to determine the temperature-dependence of their lifetime before transformation to the more stable glissile form of $\langle 111 \rangle$ crowdions [34]. Most transform in well under 1ns at temperatures in the range 500–900 K, with an activation energy of about 0.35-0.55 eV. This implies that they mainly affect the annealing of cascades rather than microstructure evolution in the long term. However, an eight-interstitial 3-D cluster did not transform in the 1ns simulations, even at 1500 K. The implications of this have not yet been considered.

Immobile arrangements of SIAs can be created in copper by similar processes to those for iron and, additionally, sessile clusters can arise because of the stability of the extrinsic stacking fault on $\{111\}$ planes, i.e. faulted Frank loops with $\mathbf{b} = 1/3\langle 111 \rangle$ can be formed in cascades. Whether the Frank loops are metastable or not with respect to the unfaulted, glissile form depends on their size and the magnitude of the fault energy. Relative stability of different SIA clusters in Cu has been studied in [35]. It was found that although perfect $1/2\langle 110 \rangle$ clusters have slightly lower formation energy, regular hexagonal Frank loops of >19 SIAs are thermally stable for at least 350ps at $T \leq 1100\text{K}$. Irregular faulted clusters and 3-D clusters are unstable and can be transformed at high T into the perfect glissile configuration. From the large number of cascades simulated in the present work, the fraction, ϵ_i^s , of the total SIA population in copper at 100K that is not glissile is plotted as a function of E_p in Fig. 8.

Non-glissile SIA clusters formed by the end of the cascade process are a mixture of sessile Frank defects and the less-specific, immobile arrangements of interstitials. In low energy cascades ($E_p \leq 10\text{keV}$), small clusters of up to about six SIAs are formed frequently and some examples are presented in Fig. 9. They can be either 3-D configurations (Figs. 9(a) and (b)) or the nuclei of faulted Frank loops (Fig. 9(c)). In higher energy cascades ($E_p = 25\text{keV}$), larger sessile and glissile SIA clusters are created quite commonly. Examples of a perfect loop of 61 SIAs, a sessile Frank loop of 59 SIAs and 3-D cluster of 18 SIAs are presented in Figs. 10, 11 and 12 respectively.

4.2. Vacancy clusters

(a) Fraction of vacancies in clusters

Most vacancies tend to form in the central region of a cascade, which is the last to regain crystalline order as the thermal spike phase comes to an end, and are therefore close to each other. It is well-known from TEM experiments that ‘collapse’ of the lattice in this region can create extended dislocation defects of vacancy type, e.g. [36,37]. However, the binding energy per vacancy of vacancy clusters is much less than that of SIAs, e.g. [31], and, furthermore, two vacancies in iron are more tightly bound in the second-nearest neighbour sites than the first. Thus, in comparison with SIAs, it is less straightforward to define unambiguously a condition for a vacancy to be a member of a cluster, particularly in the BCC case.

In early simulations of iron [14,20], vacancy clustering was analysed assuming that every vacancy in a cluster has a least another in a first-neighbour site, and this showed that the vacancy clustering fraction, ε_v , is much smaller than ε_i by a factor of about two. However, later work, e.g. [21], assessed vacancy clustering on the basis of higher-order-neighbour arrangements, with the result that ε_v can approach ε_i . The histogram in Fig. 13(a) shows the fraction of the vacancy population in clusters of a given size at 100K for cascades of 10 and 20keV in iron when defects in up to 4th-neighbour positions are defined to be clustered. (Fourth neighbour sites are separated by the vector $1/2\langle 113 \rangle$) Comparison with the SIA data in Fig. 3(a) shows that ε_v is a little smaller than ε_i , but that the population again skews towards the larger clusters with increasing E_p .

In FCC metals, where the divacancy binding energy is highest in the first-nearest neighbour configuration, it is more straightforward to use the same definition of a clustered defect as that applied for SIAs, i.e. a vacancy is a member of a cluster provided at least one other vacancy is present at a first-neighbour site. With this definition, the histograms for 10 and 25keV cascades in copper plotted in Fig. 13(b) are obtained, from which it is clear that ε_v is considerably smaller than ε_i (plotted in Fig. 3(b)). Although ε_v appears to be smaller in copper than iron, the values depend on the definitions used to identify vacancies in clusters.

It was pointed out in section 4.1(a) that MD simulations of cascades can provide quantitative information on the dependence of the fraction of clustered defects on the PKA energy spectrum. In the case of SIAs, this is important because of the change of dimensionality of migration with increasing cluster size. It is also of interest for vacancies in copper because divacancies can diffuse three-dimensionally whereas trivacancies are embryonic SFTs [18]. Thus, we present in the lower part of Fig. 6 the values for ε_v versus E_p in copper at 100 K for the cases where the minimum cluster size is either two or three vacancies. As with SIAs in the upper part of the Figure, ε_v is sensitive to the choice of minimum cluster size in the lower part of the energy spectrum.

It was seen in section 4.1(a) that the effect of increasing the ambient temperature, whilst small as far as N_F is concerned, is to increase ε_i significantly (see Fig. 4). In contrast to this, the effect on ε_v is not significant (as shown by the data for the PP model plotted in Fig. 4 of ref. [40]). This leads to a large value of $(\varepsilon_i - \varepsilon_v)$ at high irradiation temperature.

(b) The morphology of vacancy clusters

As implied by the discussion above, the clustered proportion of vacancies created by cascades in iron are in loose arrangements involving a substantial proportion of defects at sites that are not first neighbours. This leads to a marked distinction between the nature of the vacancy clusters observed in the simulated cascades in copper and iron, and reflects the situation found experimentally. Clusters in iron do not cause the surrounding crystal to collapse and form dislocation loops, even when many of the vacancies are first neighbours. This absence of loop formation by cascade collapse is consistent with TEM observations of self-ion-irradiated thin foils [36] and the evidence from positron lifetime measurements of 3-D arrangements of vacancies in neutron-irradiated iron [38]. In copper, on the other hand, extended vacancy dislocation defects formed by cascade collapse, such as loops and stacking fault tetrahedra (SFTs), are a common feature of ion- and neutron-irradiated specimens [36,39]. However, such defects were not observed systematically in previous computer simulations of cascades in copper, possibly because of the low energy range considered and the small number of cascades simulated. A preliminary report [10] on the larger data base of the present work suggested that SFTs might actually occur in simulated cascades with a size and frequency consistent with experiment. We shall therefore consider this aspect in more detail below and compare the simulation results with recent experimental data obtained from neutron-irradiated copper [39].

The vacancy clusters in the cascade simulations of copper are 3-D configurations. At low PKA energy ($< 10\text{keV}$), most clusters contain up to about eight vacancies and two types are dominant: the smallest possible SFT of three vacancies, i.e. one atom sharing four lattice sites, and highly symmetric ‘micro-voids’ of five or six vacancies. The others are simply less symmetric arrangements. Examples were presented in Fig. 5 of ref. [10]. At higher energies ($\geq 10\text{keV}$), where clusters containing more than ten vacancies commonly occur, 3-D configurations with triangular $\{111\}$ facets are often found. In fact, the majority of clusters larger than 15 vacancies are unambiguously SFT-like. They either form during the cascade thermal spike phase or transform from 3-D arrangements of vacancies into SFTs during post-cascade annealing over a period of a few tens of ps. In the latter case, the final configuration depends on the ambient temperature and simulation time. Most SFT-like structures are not regular tetrahedra, but are

either truncated or consist of more than one tetrahedron joined along a face, i.e. the number of vacancies in the cluster does not match the exact number required to form a regular SFT (10, 15, 21, 28, 36, 45, 55, ...). In the simulations carried out in the present work, the fraction of cascades that resulted in SFT-like configurations at 100K for the MBP model of copper was 0.24, 0.35 and 0.47 for 10, 20 and 25keV, respectively. Comparison of Fig. 13(b) with Fig. 3(b) shows that although more large interstitial clusters are formed in comparison with vacancy defects at the same cascade energy, the spread of size is similar. The largest SFT-like cluster formed within the cascade time scale in a 25keV cascade contained 89 vacancies: it is presented in Fig. 11. An example of an almost regular SFT containing 58 vacancies created in a cascade of the same energy is presented in Fig.14. The large vacancy defect in Fig. 11 is seen to have formed close to the 59-SIA Frank loop. Formation of large vacancy and SIA clusters in close proximity tends to be a feature of cascades in copper at all energies.

The size distribution presented at Fig.13(b) can be compared directly with the recent experimental measurements of Singh et al. [39], who measured the size and number density of SFTs in neutron-irradiated copper by transmission electron microscopy both before and after post-irradiation annealing at 573K. Their results revealed an SFT size distribution with a maximum at about 2nm and an upper limit of ~6nm. Data on vacancy clusters size distribution obtained here with the MBP for 25 keV cascades (for which we have simulated the maximum number of cascades) are presented in Fig. 13(b) and shows a maximum for large clusters in the range of 30 to 40 vacancies. The edge length, L , of a regular SFT containing N_v vacancies is $a_0\sqrt{N_v}$, where a_0 is the FCC lattice parameter. Thus, SFTs containing 30-40 vacancies in copper have L of 1.5-2nm, whereas the largest cluster found here ($N_v = 89$) would have L of about 3nm if formed as a regular SFT. Thus, the size distribution of the vacancy clusters created in the simulated cascades of the present work is qualitatively similar to that obtained in [39]. The simulated clusters were formed directly in cascades at an ambient temperature of 100K. We have not yet analysed data for higher temperature simulations for the MBP, data for the LRPP reported in [40] show an increase of the mean size of vacancy clusters at high (600K) temperature.

Three further features are relevant to the comparison of modelling with experiment. First, the stability of small SFTs is strongly size dependent, increasing for the LRPP, for example, from ~0.5 to ~0.9eV/vacancy for SFTs containing from 10 ($L = 1$ nm) to 36 ($L = 2$ nm)

vacancies, respectively [18]. Second, irregular SFTs can grow or shrink to the next regular shape when interaction with individual SIAs does not lead to an annihilation reaction [18] and therefore large SFTs are stable. Third, SFTs of ≤ 10 vacancies ($L \leq 1\text{nm}$) are not visible by transmission electron microscopy. These comments and the similarity of the experimental and simulated size distributions, lead us to conclude that the SFTs observed in as-irradiated Cu are formed directly in cascades. Further evolution of SFT size distribution observed during annealing of irradiated copper, when the maximum of the size distribution rises to $\sim 3\text{nm}$ [39], can be explained by growth of large irregular clusters to the corresponding regular tetrahedral of similar N_v . Such growth is limited due to the mechanism studied in [41] and therefore the maximum SFT size is also limited. This is different, in principle, from the evolution of vacancy clusters in the form of 3-D voids, for example, which follows a classical Ostwald ripening process. There are still problems in describing SFT evolution under irradiation, for example due to lack of knowledge of reactions between glissile SIA clusters and regular and irregular SFTs. Atomic-scale computer simulation studies of such interactions, as well as determination of the energetics of truncated SFTs, could contribute significantly to complete understanding of microstructure evolution of low stacking fault energy FCC metals under irradiation.

Conclusions

1. Results from a large number of MD simulations of displacement cascades across a wide range of primary knock-on atom energy, E_p , in both copper (FCC) and α -iron (BCC) are reviewed. The total number, N_F , of either vacancies or self-interstitial atoms created, and the fractions, ε_v and ε_i , of these defects formed in clusters are presented, and the morphology of clusters described.
2. The trends in the parameters N_F , ε_v and ε_i , can be discerned from only a few simulations at each E_p , but many simulations (~ 30 to 40) are required at each condition to reach an accuracy of about 20% in the cluster fractions because of the wide dispersion in the data.
3. N_F is smaller in copper than iron when expressed as a fraction of the NRT-predicted number because the standard value of the threshold displacement energy is smaller in copper: the absolute numbers are not widely different. N_F is not sensitive to the irradiation temperature.

4. The fraction, ϵ_i , of SIAs formed in clusters of size two or more is larger in copper than iron, and increases with increasing temperature.
5. The SIA clusters formed in cascades have a variety of forms in both metals. Most are glissile configurations of parallel crowdions and behave as perfect dislocation loops with \mathbf{b} equal to either $1/2\langle 110 \rangle$ (copper) or $1/2\langle 111 \rangle$ (iron), but a significant fraction are sessile. The latter are either three-dimensional arrangements, most of which transform to the glissile form during post-cascade annealing, or, in copper, Frank dislocation loops with $\mathbf{b} = 1/3\langle 111 \rangle$. Out of 53 cascades of 25keV in copper at 100K, the largest Frank loop contained 59 SIAs. The largest perfect loop found contained 61 SIAs.
6. Tightly-packed arrangements of vacancies do not form in iron under the conditions studied and ϵ_v for vacancies in clusters of size two or more is strongly dependent on the range of neighbour shells within which the defects are defined to form a cluster. In copper, in contrast, the same definition of clustering as used for SIAs, i.e. defects in first-neighbour sites, shows that although ϵ_v is smaller than ϵ_i , vacancy clusters are common and large.
7. The vacancy clusters in copper are three-dimensional in form and, for E_p values above about 10keV, most have triangular $\{111\}$ facets, i.e. they are irregular stacking fault tetrahedral (SFTs). In 53 simulations of cascades of 25keV at 100K, the largest such cluster formed contained 89 vacancies and the largest near-regular SFT contained 58 vacancies. There is a correlation in the formation of large vacancy and SIA clusters, for they tend to occur in the same cascade in close proximity to each other.
8. The size spectrum of the SFT-like clusters created in these 53 simulations is similar to that found in recent experiments on neutron-irradiated copper [39], leading to the conclusion that the SFTs observed in experiment are formed directly in the core of cascades as part of the primary damage state.

Acknowledgements

This research was supported by a grant from the UK Engineering and Physical Sciences Research Council, a JREI grant from the Higher Education Funding Council for England, and grant FIKS-CT-2001-00137 (SIRENA) from the Council of the European Commission.

References

1. D.J. Bacon and T. Diaz de la Rubia, *J. Nucl. Mater.* 216 (1994) 275.
2. D.J. Bacon, A.F. Calder, F. Gao, V.G. Kapinos and S.J. Wooding, *Nucl. Instrum. and Meth. B* 102 (1995) 37.
3. D.J. Bacon, A.F. Calder and F. Gao, *J. Nucl. Mater.* 251 (1997) 1.
4. D.J. Bacon, F. Gao and Yu.N Osetsky, *J. Computer-Aided Mater. Des.* 6 (1999) 225.
5. B.N. Singh, S.I. Golubov, H. Trinkaus, A. Serra, Yu.N. Osetsky and A.V. Barashev, *J. Nucl. Mater.* 251 (1997) 107.
6. S.I. Golubov, B.N. Singh, H. Trinkaus, *J. Nucl. Mater.* 276 (2000) 78.
7. M. Kiritani, T. Yoshie, S. Kojima, *J. Nucl. Mater.* 141-143 (1986) 625.
8. A. Calder, D.J. Bacon, W.J. Phythian, C.A. English, *Mater. Sci. Forum* 97-99 (1992) 183.
9. T.L. Daulton, M.A. Kirk, L.E. Rehn, *Philos. Mag. A* 80 (2000) 809.
10. Yu.N. Osetsky and D.J. Bacon, *Nucl. Instrum. and Meth. B* 180 (2001) 85.
11. C.C. Matthai, D.J. Bacon, *J. Nucl. Mater.* 135 (1985) 173.
12. V.G. Kapinos, Yu.N. Osetsky, P.A. Platonov, *Soviet Phys. Solid State* 28 (1986) 3603.
13. V.G. Kapinos, Yu.N. Osetsky, P.A. Platonov, *J. Nucl. Mater.* 165 (1989) 286.
14. W.J. Phythian, R.E. Stoller, A.J.E. Foreman, A.F. Calder, D.J. Bacon, *J. Nucl. Mater.* 223 (1995) 245.
15. G.J. Ackland, G. Tichy, V. Vitek, M.W. Finnis, *Philos. Mag. A* 56 (1987) 735.
16. Yu.N. Osetsky, A.G. Mikhin, A. Serra, *Philos. Mag. A* 72 (1995) 361.
17. J.P. Biersack, *Nucl. Inst. and Meth. B* 27 (1987) 21.
18. Yu.N. Osetsky, A. Serra, M. Victoria, S.I. Golubov and V. Priego, *Philos. Mag., A* 79 (1999) 2259.
19. M. W. Finnis and J. E. Sinclair, *Phil. Mag. A* 50 (1984) 45.
20. A. F. Calder and D. J. Bacon, *J. Nucl. Mater.* 207 (1993) 22.
21. R.E. Stoller, *J. Nucl. Mater.* 276 (2000) 22.
22. Yu.N. Osetsky, unpublished.
23. M. J. Norgett, M. T. Robinson and I. M. Torrens, *Nucl. Eng. Design* 33 (1975) 50.
24. F. Gao, D.J. Bacon, P.E.J. Flewitt and T.A. Lewis, *J. Nucl. Mater.* 249 (1997) 77.
25. F. Gao, D.J. Bacon, L.M. Howe and C.B. So, *J. Nucl. Mater.* 294 (2001) 288.
26. F. Gao and D.J. Bacon, *Phil. Mag. A* 80 (2000) 1453.

27. B.D. Wirth, G.R. Odette, D. Maroudas and G.E. Lucas, *J. Nucl. Mater.* 244 (1997) 185.
28. N. Soneda and T. Diaz de la Rubia, *Phil. Mag. A* 78 (1998) 995.
29. Yu.N. Osetsky, A. Serra, V. Priego, F. Gao and D.J. Bacon, in *Diffusion Mechanisms in Crystalline Solids*, eds. Y. Mishin et al., Symp. Proc. vol. 527 (MRS Pittsburgh, 1998) p. 49 and p. 59.
30. Yu.N. Osetsky, D.J. Bacon and A. Serra, *Phil. Mag. Lett.* 79 (1999) 273.
31. Yu.N. Osetsky, D.J. Bacon, A. Serra, B.N. Singh and S.I. Golubov, *J. Nucl. Mater.* 276 (2000) 65.
32. Yu.N. Osetsky, D.J. Bacon, A. Serra, B.N. Singh and S.I. Golubov, *Philos. Mag., A*, 83 (2003) 61.
33. A.V. Barashev, Yu.N. Osetsky and D.J. Bacon, *Phil. Mag. A* 80 (2000) 2709.
34. F. Gao, D.J. Bacon, Yu.N. Osetsky, P.E.J. Flewitt and T.A. Lewis, *J. Nucl. Mater.*, 276 (2000) 213.
35. Yu.N. Osetsky, D.J. Bacon, A. Serra, B.N. Singh and S.I. Golubov, *Philos. Mag., A*, 80 (2000) 2131
36. C.A. English and M.L. Jenkins, *Mater. Sci. Forum* 15-18 (1987) 1003.
37. C.A. English, A.J.E. Foreman, W.J. Phythian, D.J. Bacon and M.L. Jenkins, *Mater. Sci. Forum* 97-99 (1992) 1.
38. M. Eldrup and B.N. Singh, *J. Nucl. Mater.*, 276 (2002) 269.
39. B.N. Singh, D.J. Edwards and P. Toft, *J. Nucl. Mater.*, 299 (2001) 205.
40. Yu.N. Osetsky, D.J. Bacon and B.N. Singh, *J. Nucl. Mater.*, 307-311 (2002) 866.
41. Yu.N. Osetsky, A. Serra, M. Victoria, V. Priego and S.I. Golubov, *Philos. Mag., A* 79, 2285 (1999).

FIGURE CAPTIONS

- Fig. 1. Number of surviving vacancy or SIA defects, N_F , averaged for each PKA energy, divided by the NRT-predicted number, N_{NRT} , as obtained by computer simulation for iron and copper (MBP) at 100K. The bars are the standard error (SE). The NRT values are calculated with $E_d = 30\text{eV}$ for copper and 40eV for iron.
- Fig. 2. Number of surviving vacancy or SIA defects, N_F , averaged for each PKA energy, as obtained by computer simulation for (a) iron and (b) copper (MBP) at 100K. The small and large bars show the SE and standard deviation (SD), respectively. The number in parentheses in (b) is the number of cascades simulated at that condition.
- Fig. 3. Histograms showing the size distribution of SIA clusters created at 100K by (a) 10 and 50keV cascades in iron and (b) 10 and 25keV cascades in copper (MBP). The fraction of SIAs in clusters of size larger than the maximum shown is denoted by Σ .
- Fig. 4. The fraction, ε_i , of SIAs formed in clusters where every defect has at least one first-nearest neighbour in copper modelled with the PP at either 100 or 600K. (Bars show the SE.)
- Fig. 5. The fraction, ε_i , of SIAs formed in clusters where every defect has at least one first-nearest neighbour in copper modelled at 100K with either the MBP or the PP. (Bars show the SE.)
- Fig. 6. The fraction of defects in copper at 100 K that survive in SIA clusters of two or more, three or more, and four or more (upper plot) and vacancy clusters of two or more, and three or more (lower plot).
- Fig. 7. The fraction of SIAs formed in clusters formed in a metastable sessile configuration by the end of the thermal spike phase as a function of PKA energy and irradiation temperature for cascades in α -iron [34]. (Bars show the SE.)
- Fig. 8. The fraction of SIAs formed in clusters in a metastable sessile configuration by the end of the thermal spike phase as a function of PKA energy for cascades in copper (MBP) at 100K. (Bars show the SE.)
- Fig. 9. Examples of configurations of SIA clusters observed in 5 and 10keV cascades in copper simulated at 100K [10]. Dark spheres are atoms in interstitial positions, light spheres are vacant sites.

- Fig.10. Perfect glissile loop of 61 SIAs formed by a 25keV cascade in copper at 100K. The loop is shown in $\langle 110 \rangle$ projection, the direction of its Burgers vector in (a) and in the orthogonal $\langle 1\bar{1}0 \rangle$ projection in (b). Dark spheres are atoms in interstitial positions, light spheres are vacant sites.
- Fig. 11. Large SIA and vacancy clusters formed by a 25keV cascade in copper at 100K. The cluster on the right is a sessile Frank loop of 59 SIAs. That on the left is a 3-D SFT-like cluster of 89 vacancies. Light spheres are atoms in interstitial positions, dark spheres are vacant sites.
- Fig. 12. A sessile 3-D cluster of 18 SIAs formed by a 25keV cascade in copper at 100K. Light spheres are atoms in interstitial positions, dark spheres are vacant sites.
- Fig. 13. Histograms showing the size distribution of vacancy clusters created at 100K by (a) 10 and 20keV cascades in iron and (b) 10 and 25keV cascades in copper (MBP). A vacancy in a cluster has at least one other within the first four neighbour shells in (a) or at a first neighbour position in (b). The fraction of vacancies in clusters of size range indicated is denoted by Σ .
- Fig. 14. The largest near-regular SFT-like vacancy cluster formed by a 25keV cascade in copper (MBP) at 100K. It contains 64 vacancies and has an edge length of ~ 2.5 nm. A regular SFT of this size would contain 45 vacancies. Light spheres are atoms in interstitial positions, dark spheres are vacant sites.

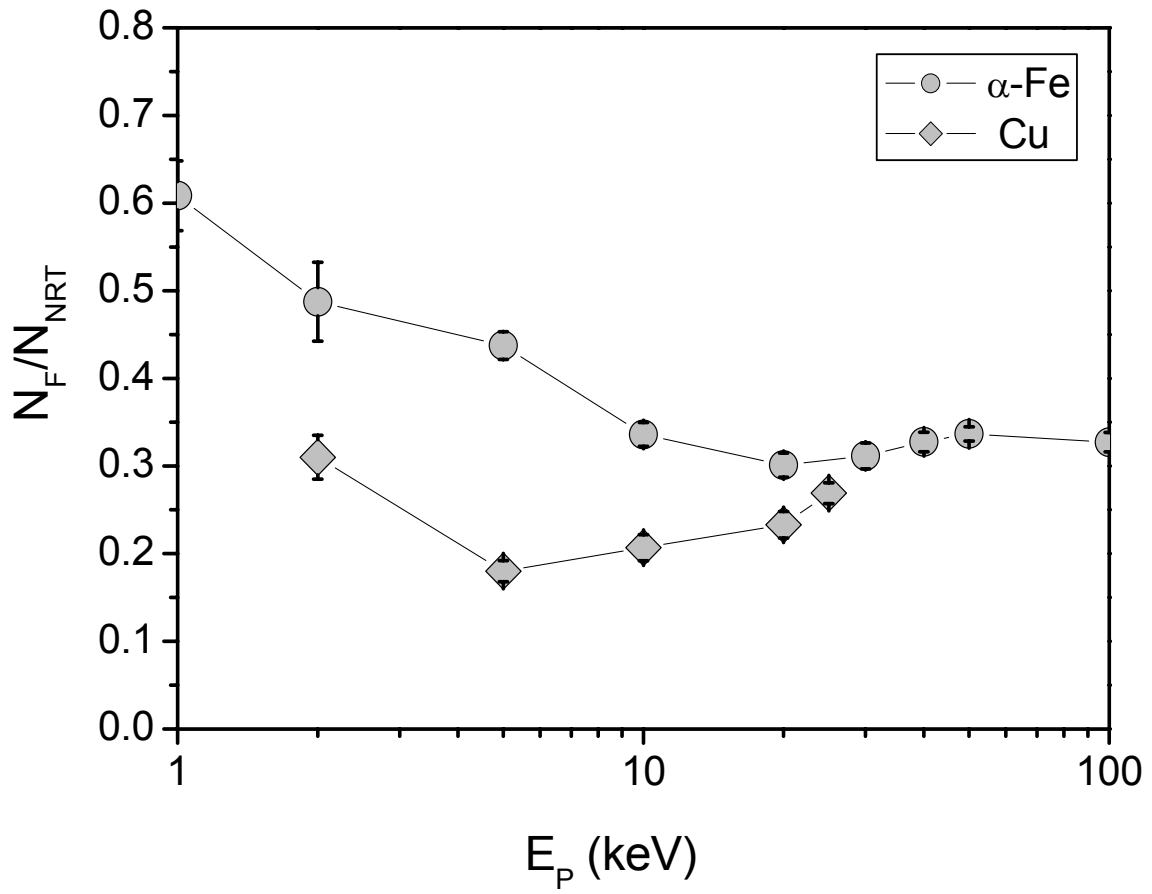


Fig.1

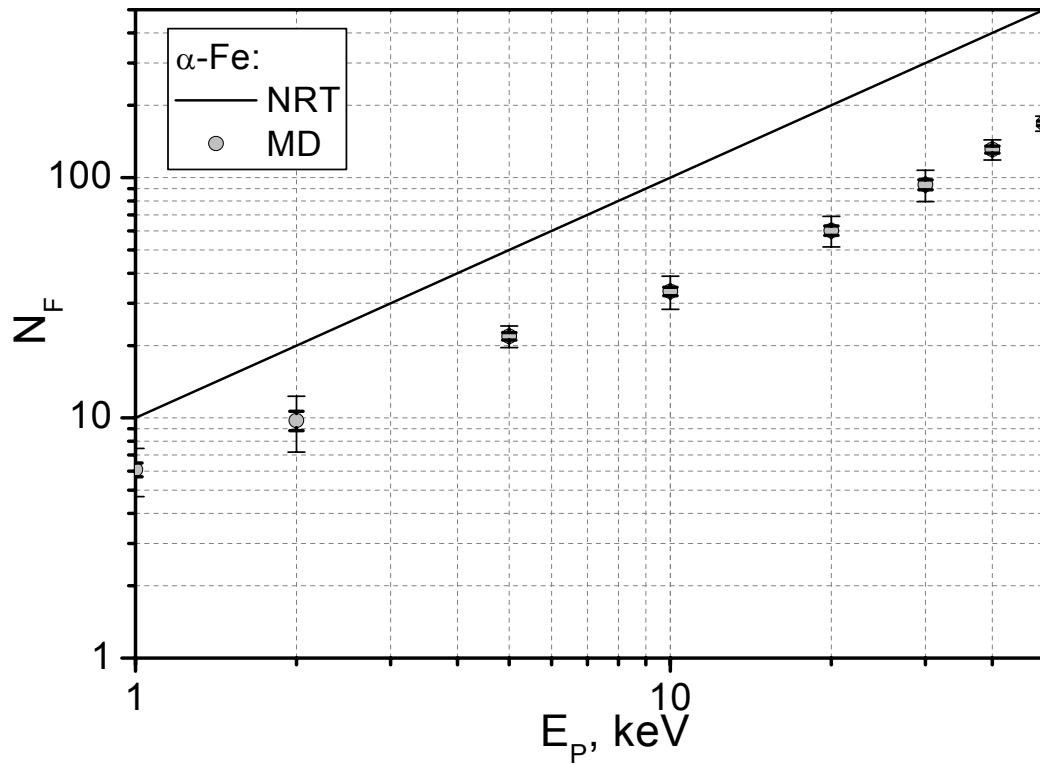


Fig.2a

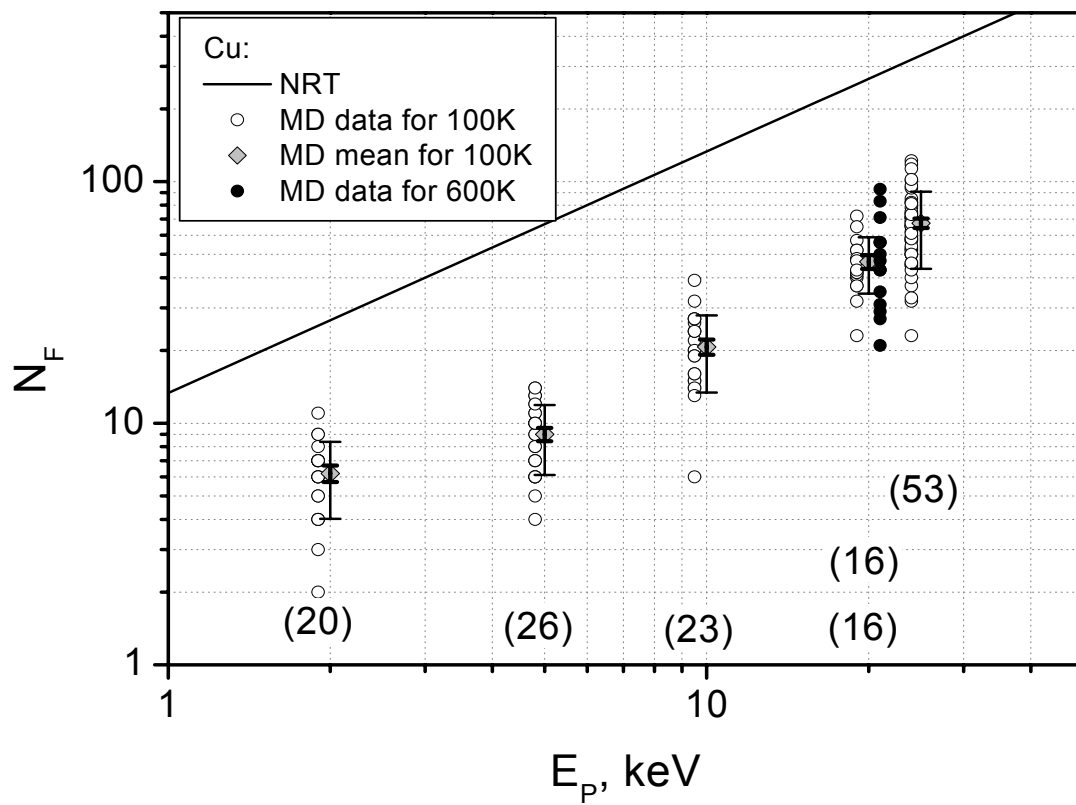


Fig.2b

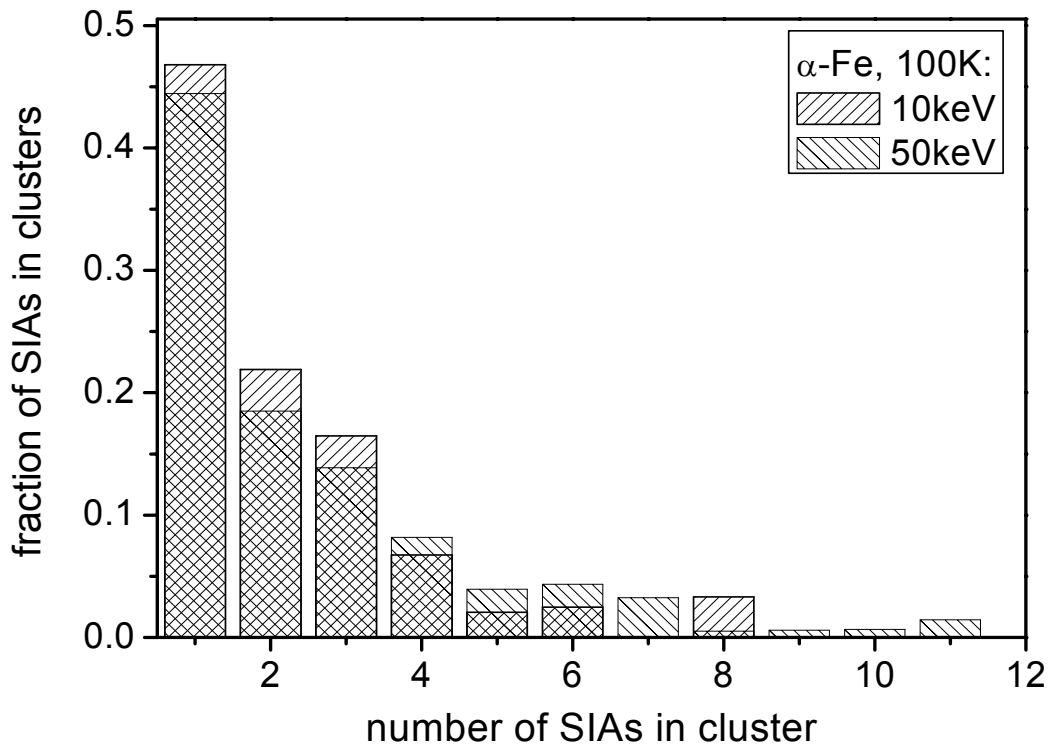


Fig.3a

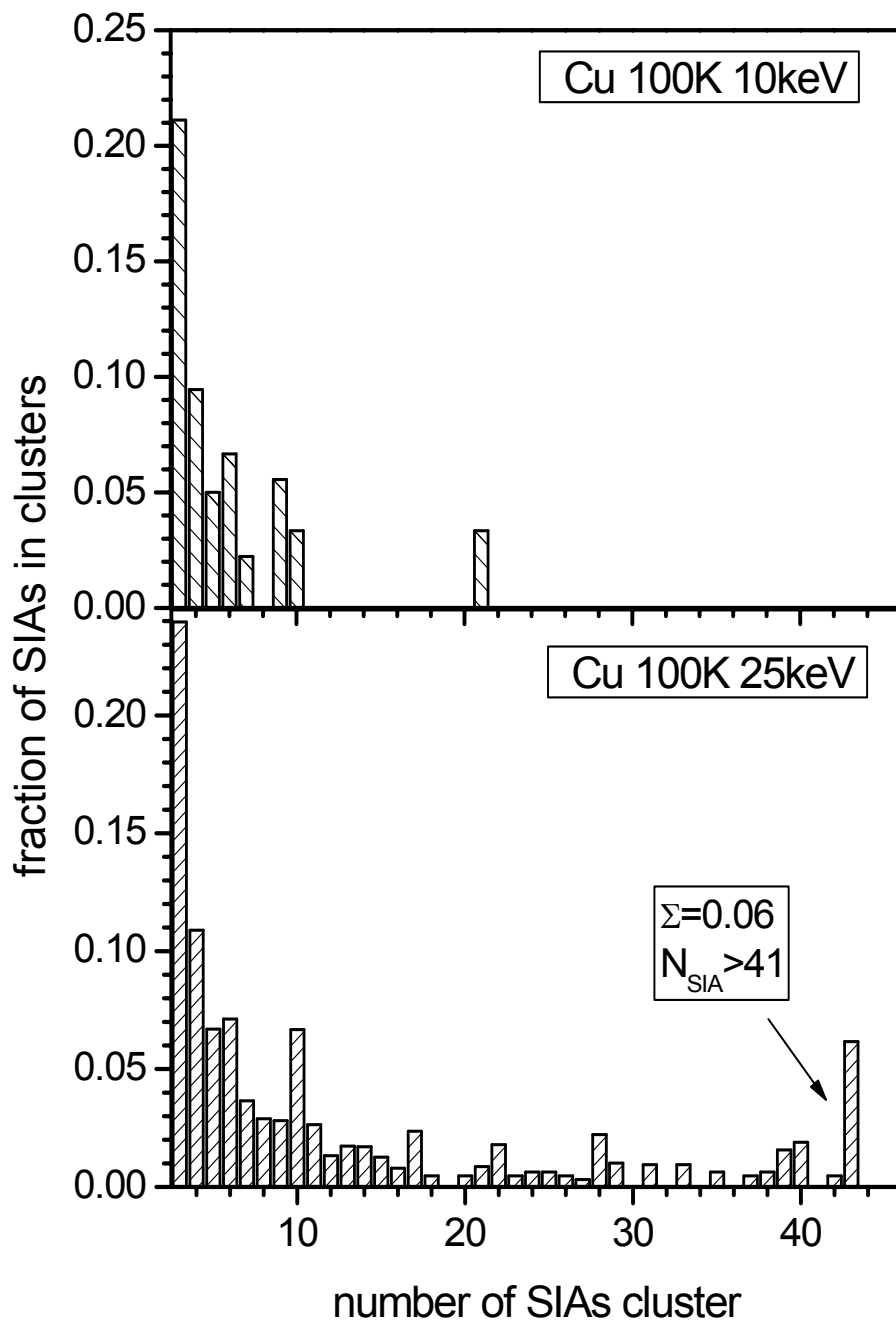


Fig.3b

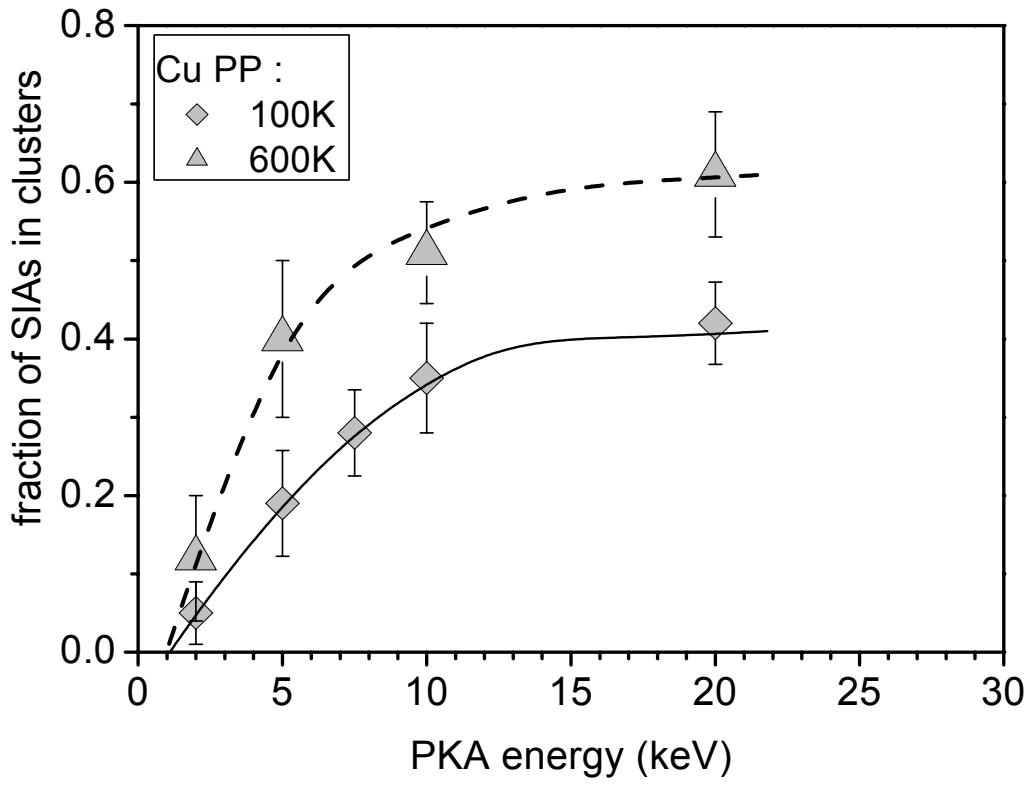


Fig.4

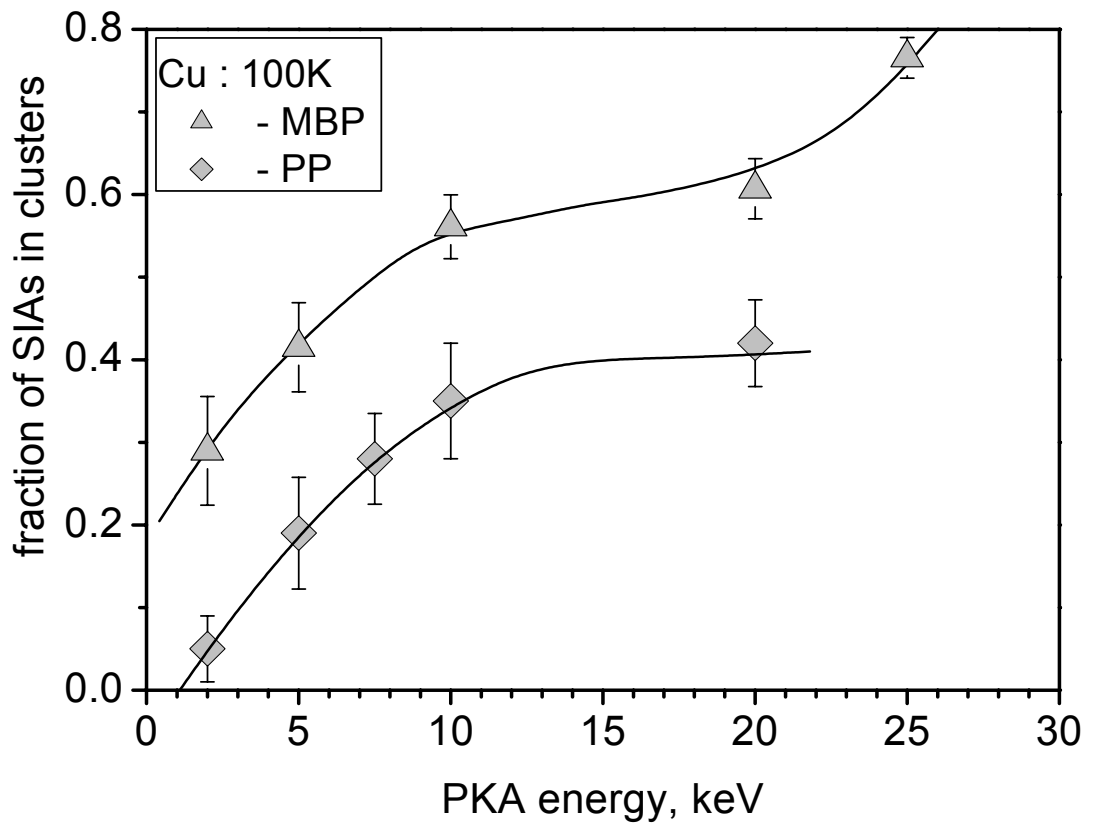


Fig.5

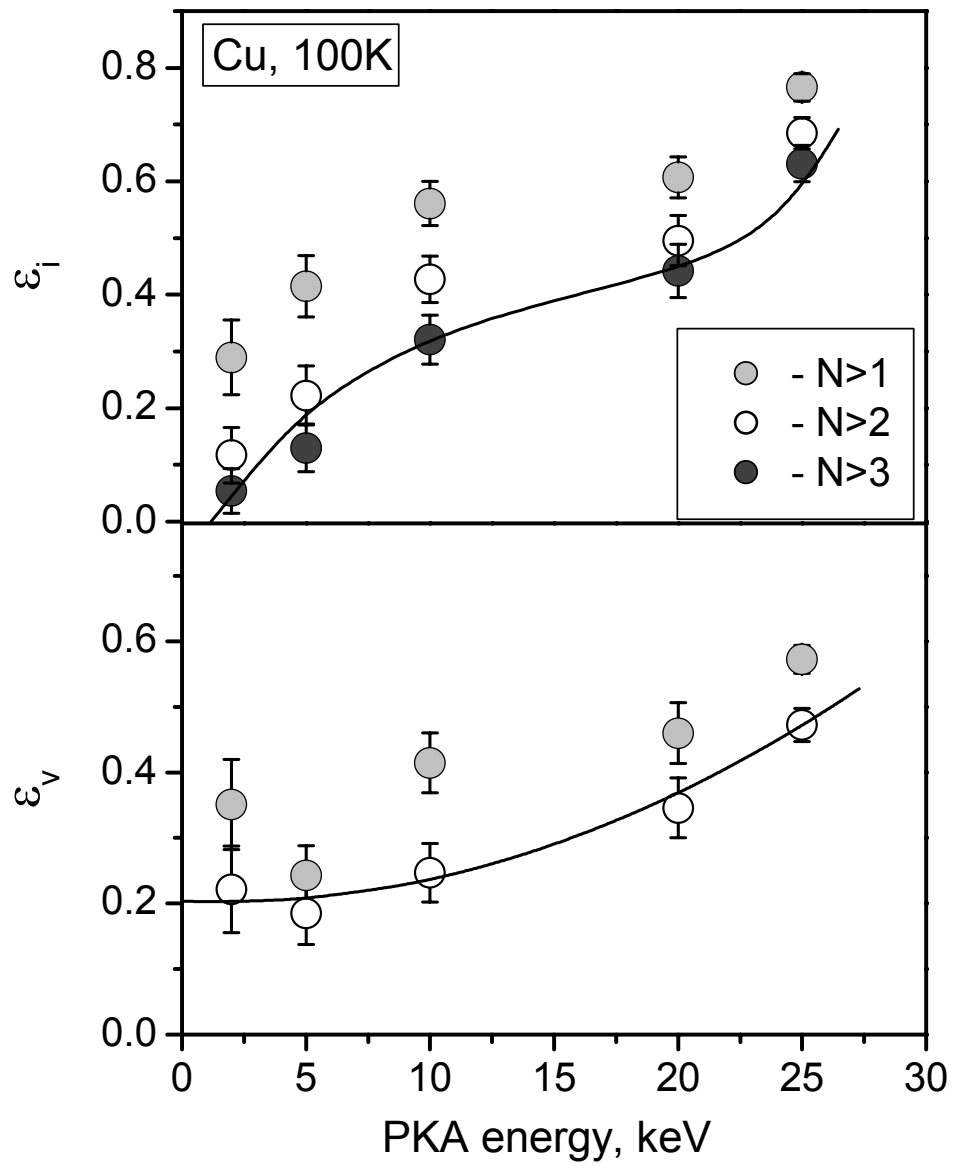


Fig.6

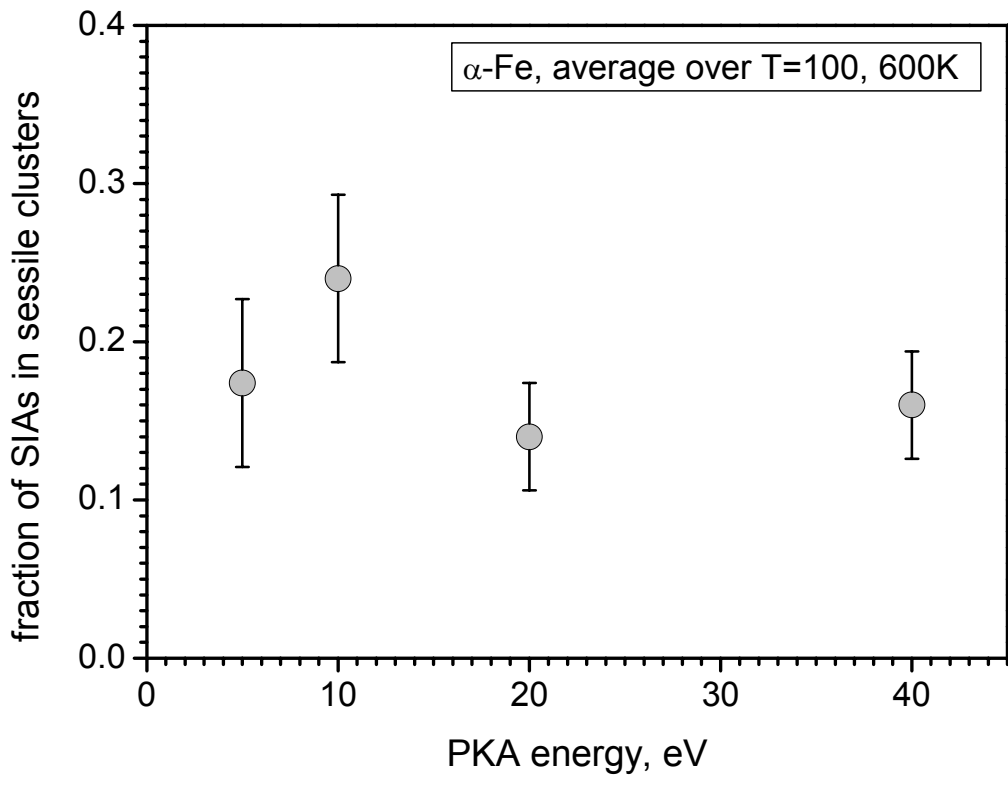


Fig.7

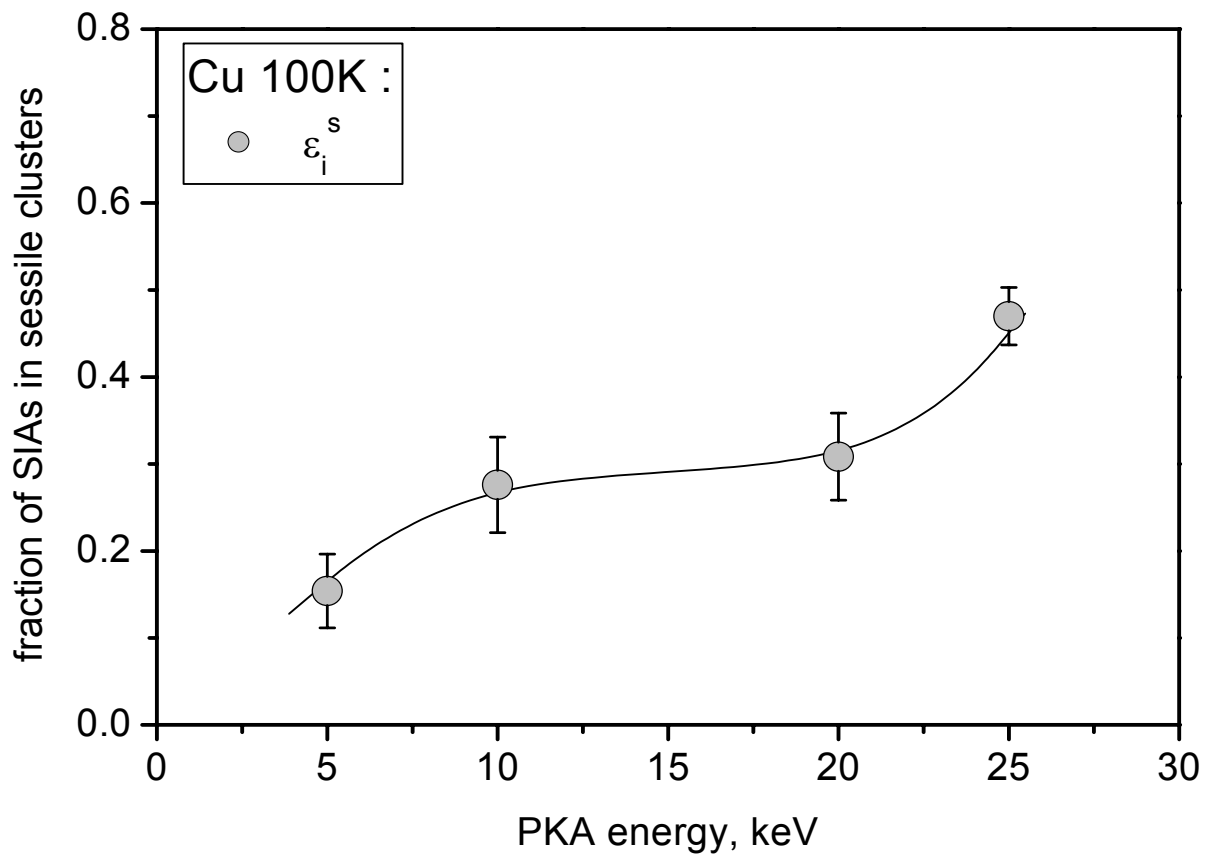


Fig.8

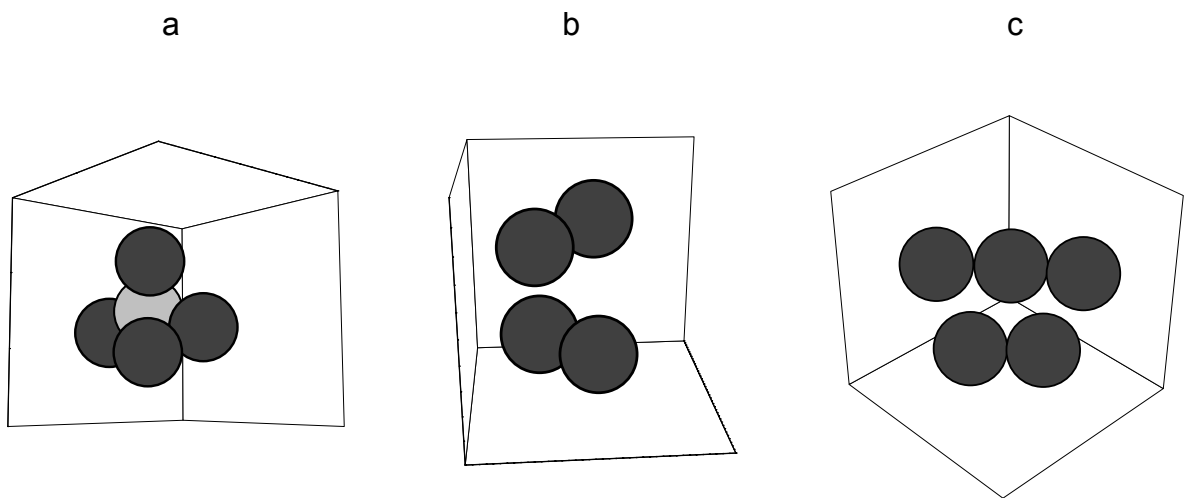


Fig.9

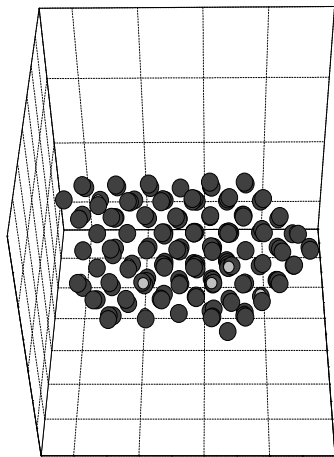


Fig.10a

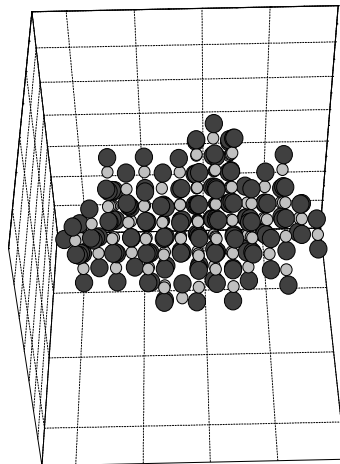


fig.10b

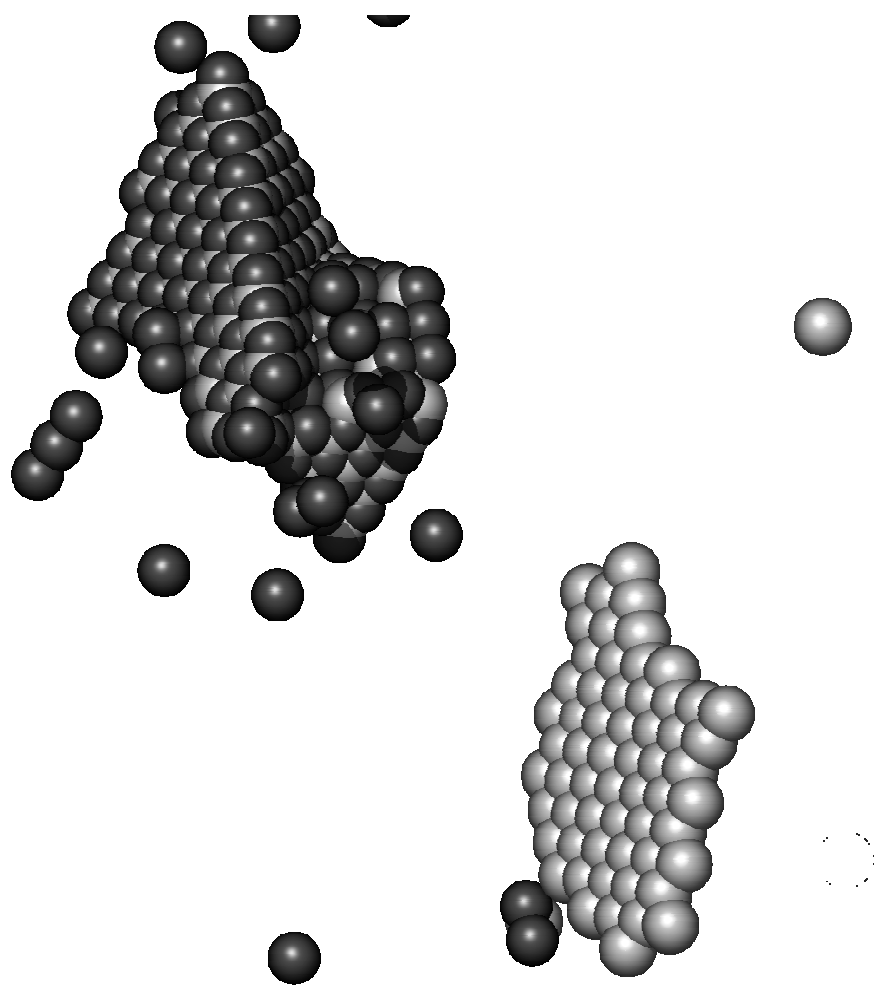


Fig.11

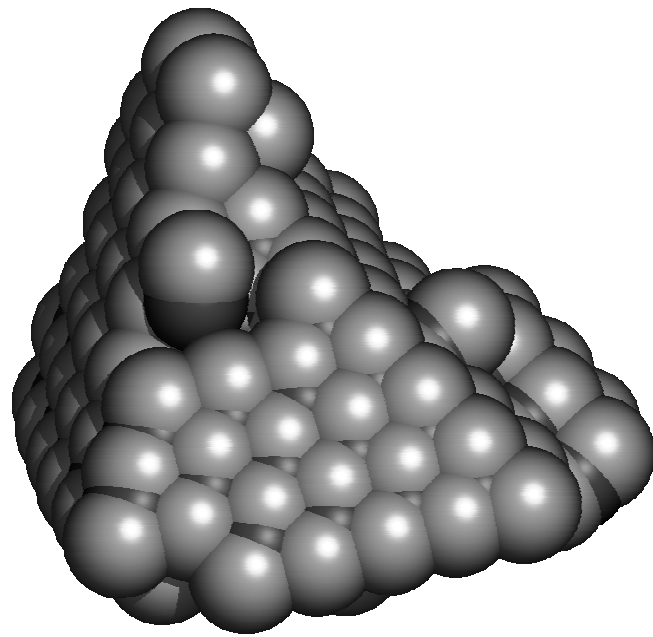


Fig.12

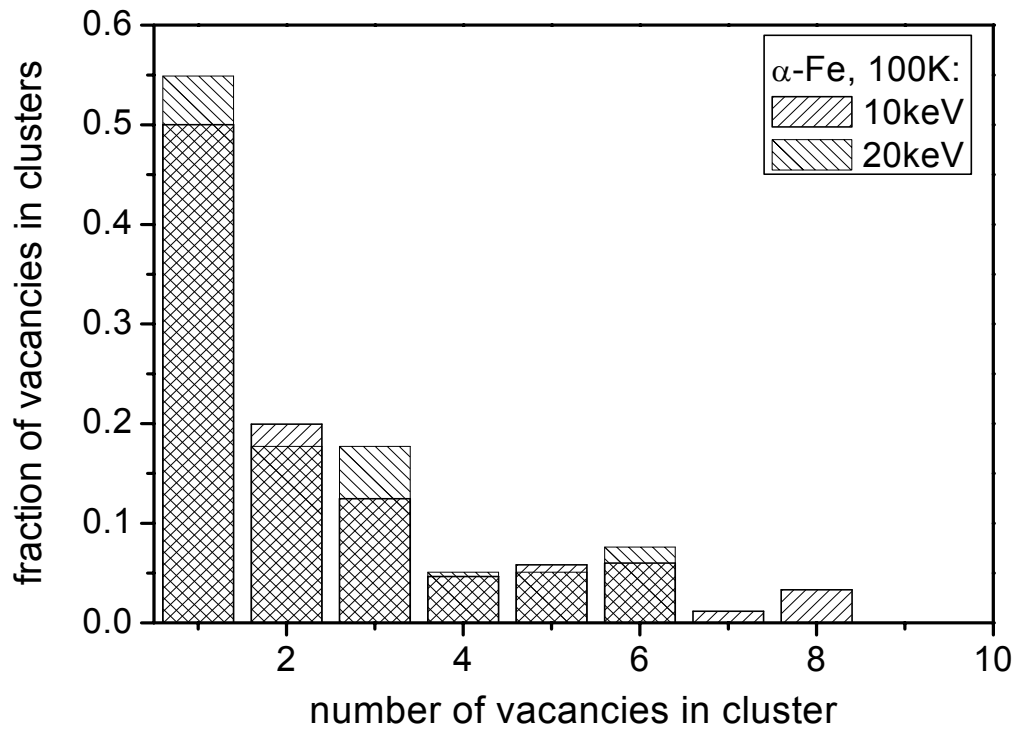


Fig.13a

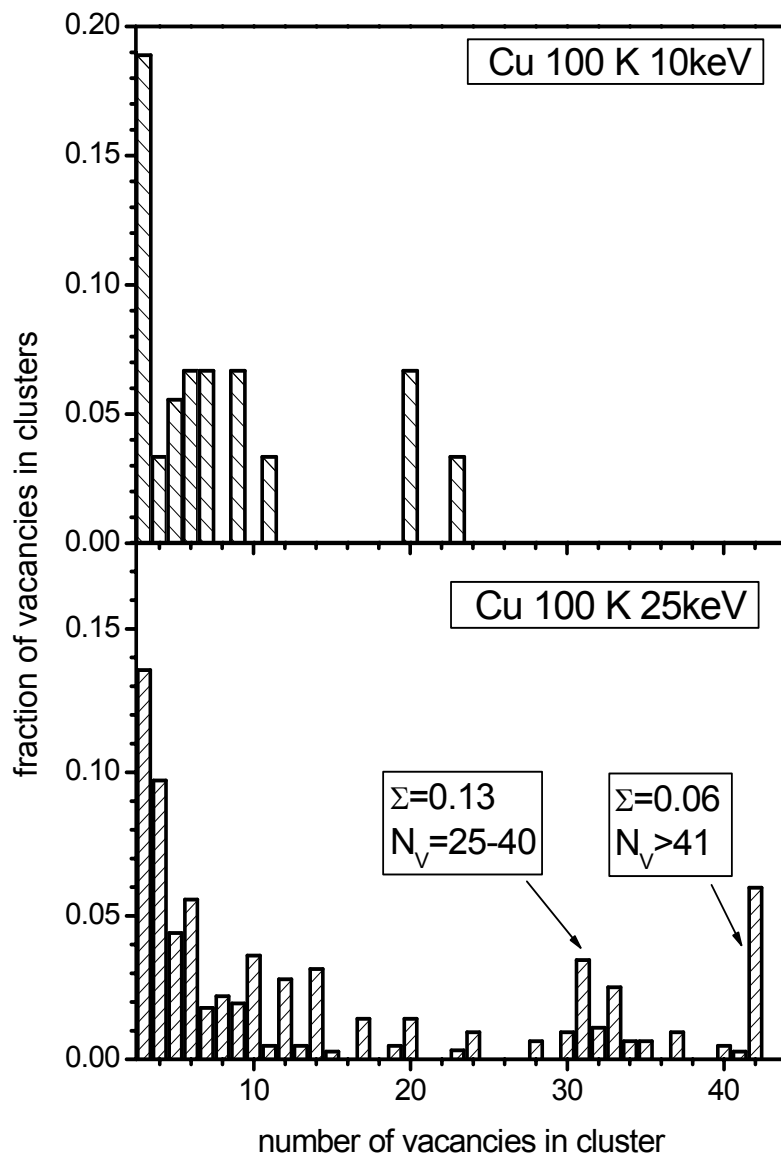


Fig.13b

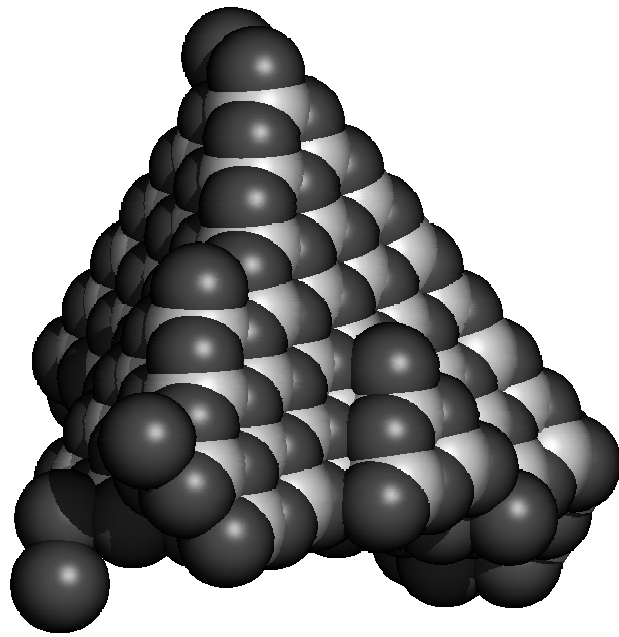


Fig.14